First Evidence of Purely Extreme-Ultraviolet Four-Wave Mixing

L. Foglia,[1,*] F. Capotondi,[1] R. Mincigrucci,[1] D. Naumenko,[1] E. Pedersoli,[1] A. Simoncig,[1] G. Kurdi,[1] A. Calvi,[2] M. Manfredda,[1] L. Raimondi,[1] N. Mahne,[3] M. Zangrando,[1,3] C. Masciovecchio,[1] and F. Bencivenga[1]
[1]*Elettra-Sincrotrone Trieste S.C.p.A., S.S. 14 km 163.5 in Area Science Park, I-34012 Basovizza, Trieste, Italy*
[2]*Department of Physics, University of Trieste, Via A.Valerio 2, 34127 Trieste, Italy*
[3]*IOM-CNR, Strada Statale 14-km 163.5, 34149 Basovizza, Trieste, Italy*

(Received 8 January 2018; published 26 June 2018)

The extension of nonlinear optical techniques to the extreme-ultraviolet (EUV), soft and hard x-ray regime represents one of the open challenges of modern science since it would combine chemical specificity with background-free detection and ultrafast time resolution. We report on the first observation of a four-wave-mixing (FWM) response from solid-state samples stimulated exclusively by EUV pulses. The all-EUV FWM signal was generated by the diffraction of high-order harmonics of the FERMI free-electron laser (FEL) from the standing wave resulting from the interference of two crossed FEL pulses at the fundamental wavelength. From the intensity of the FWM signal, we are able to extract the first-ever estimate of an effective value of $\sim 6 \times 10^{-24}$ $m^2\ V^{-2}$ for the third-order nonlinear susceptibility in the EUV regime. This proof of principle experiment represents a significant advance in the field of nonlinear optics and sets the starting point for a manifold of techniques, including frequency and phase-resolved FWM methods, that are unprecedented in this photon-energy regime.

DOI: 10.1103/PhysRevLett.120.263901

Nonlinear optical (NLO) spectroscopies have become well established techniques in the visible and near infrared photon-energy range for the investigation of a large variety of fundamental processes, such as vibrational, electron, and spin dynamics or structural properties, with energy, momentum, and ultrafast time resolution. They result from the interaction of the Nth-order nonlinear susceptibility with strong incident electric fields, in what is called an $(N+1)$-wave-mixing mechanism [1]. The ability of controlling parameters such as frequency, intensity, polarization, arrival time, and angle of incidence for each field independently gives rise to an enormous variety of potential experimental techniques, mostly limited by technical issues only. In fact, the development of NLO spectroscopies went hand in hand with the evolution of tabletop laser systems providing tunable, coherent, ultrashort, and reproducible waveforms. Similarly, the increasing availability of free-electron laser (FEL) sources, which are capable of delivering remarkably bright extreme ultraviolet (EUV) to x-ray pulses with coherence properties similar to those of optical lasers, has stimulated the scientific community towards the extension of NLO to this energy and wave vector range. EUV and x-ray NLO enables improving the spatial resolution to the nanometer range and exploiting core resonances to achieve elemental selectivity [2–5]. This, combined with the multiwave nature of the NLO approach, will allow gaining information inacessible by "conventional" (linear) experiments, such as electronic correlations and ultrafast charge flows among different atoms in a sample. Thus far, these capabilities have been envisioned, and thoroughly discussed, only theoretically [3,6–8]. Indeed, to date, the experimental approach remains limited to a few pioneering works on parametric down-conversion [9], stimulated [10] and amplified spontaneous emission [11], two photon absorption [12], nonlinear Compton scattering [13], second harmonic generation [14], EUV and visible sum frequency generation [15], and EUV stimulated but optically probed transient grating (TG) [16,17]. The latter belongs to the four-wave-mixing (FWM) processes, where three coherent beams of wavelength λ_i and momentum $\mathbf{k}_i$ $(i = 1, 2, 3)$ interact at a crossing angle 2θ on the sample via the third-order susceptibility $\chi^{(3)}$ to generate a signal beam of wavelength $1/\lambda_s = 1/\lambda_1 - 1/\lambda_2 + 1/\lambda_3$ and momentum $\mathbf{k}_s = \mathbf{k}_1 - \mathbf{k}_2 + \mathbf{k}_3$, the so-called phase matching condition [1,18]. Since $\chi^{(3)}$, unlike $\chi^{(2)}$ and all even-order NLO susceptibilities, does not vanish in centrosymmetric systems, FWM processes are the most common NLO interactions in nature and the kind of processes considered mainly by theoreticians. In addition to TG, they include, among others, the optical Kerr effect, coherent Raman scattering, multidimensional spectroscopy, and impulsive stimulated Rayleigh, Brillouin, and Raman scattering.

In this Letter we report on a significant advance in EUV NLO: the very first experimental evidence of a four-wave-mixing response stimulated purely by EUV pulses. The FWM signal is generated by the scattering of copropagating FEL harmonics from the TG formed upon interference of FEL pulses at the fundamental wavelength. The experiment takes advantage of the unique properties of the seeded

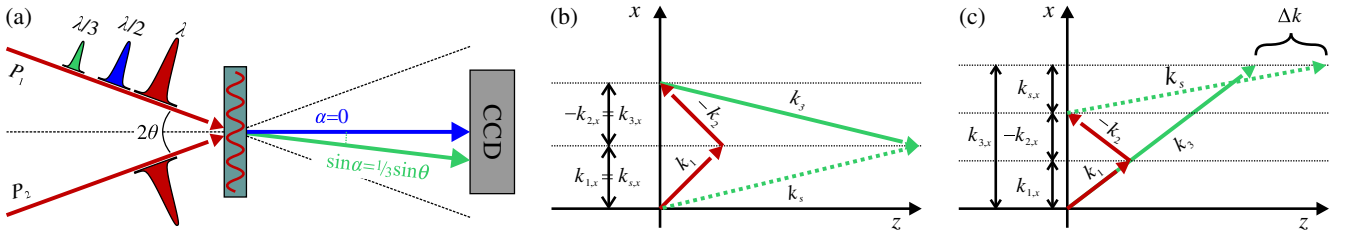

FIG. 1. (a) Scheme of the experimental setup. Pumps P_1 and P_2 of wavelength λ impinge on the sample to generate a transient interference pattern. The FEL harmonics $\lambda/2$ and $\lambda/3$, both propagating collinear and time coincident with P_1, are scattered by this transient grating and impinge on the CCD detector at the bisector of the crossing angle 2θ and at an angle α defined by $\sin\alpha = 1/3\sin\theta$, respectively. (b) Scheme of the perfect phase matching condition, where scattering occurs at the Bragg angle θ_B only (see the text). (c) Phase matching condition for thin gratings, where only the x component of the momentum is conserved and scattering is possible for an arbitrary angle of incidence. Indicated is the wave vector mismatch Δk along z.

FERMI FEL [19,20], which generates quasi–transform-limited pulses (20–60 fs) tunable in the 20 to 300 eV energy range, with a few tens of meV bandwidth and full polarization control [21]. Moreover, FERMI is capable of emitting in multicolor schemes, in addition to the copropagating high-order harmonics that intrinsically accompany FEL emission, in the "twin-seed mode" [20,22,23] or tuning one section of the undulators to different harmonics [24] or, finally, employing the double cascade configuration of FEL 2. These multicolor emission strategies have been exploited in the present experiment, as shown in Fig. 1(a): Two FEL beams, called the pump, at the fundamental wavelength $\lambda = \lambda_1 = \lambda_2$ interact on the sample at the crossing angle 2θ to generate a stationary interference pattern with periodicity $\Lambda = 2\pi/|\mathbf{k}_{ex}| = \lambda/(2\sin\theta)$, along $\mathbf{k}_{ex} = \mathbf{k}_1 - \mathbf{k}_2$. This, in turn, behaves as a transient diffraction grating for the third pulse of wavelength $\lambda_3 = \lambda/2$ or $\lambda/3$, propagating collinear with one of the pump beams and intrinsically overlapped in space and time, as shown in Fig. 1. Their interaction leads to the scattering of a signal beam at the probe wavelength at the bisector of the crossing angle or at an angle defined by $\sin\alpha = (\sin\theta)/3$, respectively. This differs from optical TG experiments in transparent materials, where the signal intensity is appreciable only at the Bragg angle $\theta_B = \arcsin(\lambda/2\Lambda)$ since the light absorption length is typically much larger than the grating period and the TG is equivalent to a thick volume grating. Instead, the Bragg condition, corresponding to the diagram in Fig. 1(b), can be strongly relaxed in the limit of thin gratings, i.e., when the thickness of the grating is on the order of the grating period Λ or smaller. Then, only the momentum component parallel to the sample surface is conserved and diffraction is possible for an arbitrary angle of incidence of the probe beam, thus effectively allowing the exploited experimental geometry. This situation is sketched in Fig. 1(c), and, clearly, conservation of the parallel momentum component only leads to a wave vector mismatch $\Delta\mathbf{k}$, which contributes to the effective coherence built-up length L_C of the NLO process as $L_C = 2/\Delta\mathbf{k}$. In the general case, the diffracted signal intensity depends on the balance of L_C and the interaction length of the pulses L as $L^2\beta$, where $\beta = \mathrm{sinc}^2(L/L_C)$ [1]. In other words, a large Δk is equivalent to a reduced sample volume for the coherent addition of the FWM signal and, therefore, can strongly decrease the process efficiency in samples with a potentially large interaction volume. However, typical absorption lengths for EUV light in solids are comparable to such coherence lengths and FWM can be observed even for a significant Δk. That said, among all possible FWM processes resulting from the intrinsic time and space overlap of both FEL harmonics with the fundamental, the reported one results in the smaller wave vector mismatch and the highest intensity. Furthermore, the other processes would fall outside the range subtended by the detector.

The experiment was performed at the EIS-TIMER end station, a beam line purposely conceived to perform all-EUV FWM experiments. Its optical transport is based on a fully reflective scheme, explained in detail elsewhere [25–28], where the FEL beam is split geometrically by removable wave front division beam splitters. Briefly, a plane mirror divides the beam along the horizontal plane into two halves, which can be recombined with four possible crossing angles of $2\theta = 18.4°$, 27.6°, 79°, and 105.4°. The data presented here were obtained using the second configuration. Each beam half contains both the fundamental wavelength pulses, used as pump, and the copropagating harmonics, used as probe. Transmission of the probe along one of the pump paths, hereafter called path 2, is avoided by using a 100 nm Mg filter sandwiched in two films of 50 nm of Al, while the other pump and the probe pulse follow path 1. FEL pump-optical probe transient transmission experiments with an external laser were used to determine the temporal overlap between paths 1 and 2. The pump pulses and the harmonics are intrinsically time overlapped at the source. The intensity of the FEL pulses was measured in ionization chambers along the beam transport [29], using a 200 nm Al or 100 nm Zr filter to select only the fundamental or the third harmonic, respectively. The signal was detected by a charge coupled device (CCD, Princeton Instruments PI-MTE) placed along the scattering direction 19 cm from the sample, and the images were acquired with a 2×2 pixel binning. A 150 nm Zr filter was used in front of the detector to reduce the background counts due to the diffusive scattering at the

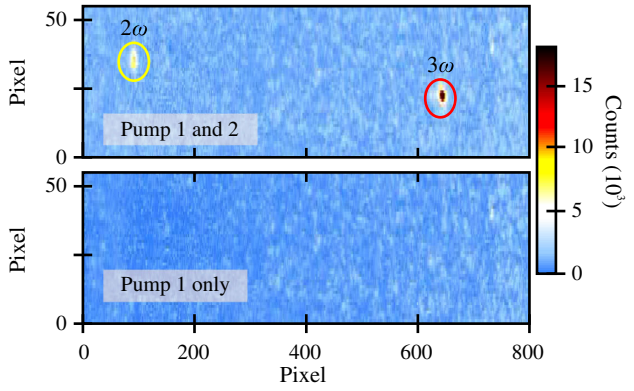

FIG. 2. (a) CCD image of signal spots due to the scattering of the second and third harmonic FEL beams that propagate collinearly with pump 1. The image is recorded with both pump beams incident on the sample. (b) Image of the same CCD region when pump 2 is blocked. The disappearance of the signal indicates that it correlates with the presence of both pump beams, as expected for FWM.

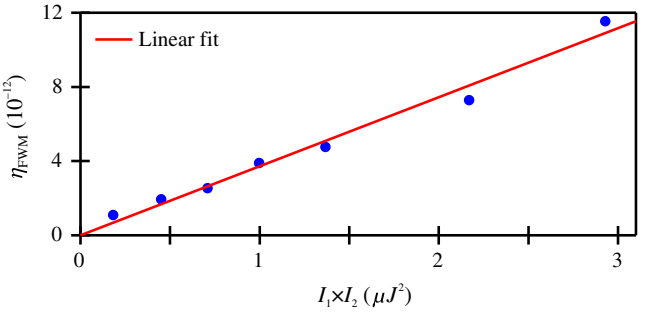

FIG. 3. FWM efficiency η_{FWM} plotted as a function of the product of pump 1 and 2 energies in μJ. The solid (red) line indicates a linear fit, thus confirming that the observed signal is indeed due to FWM.

fundamental wavelength well below the appreciable signal to noise level. Images were acquired for 1 min at a FEL repetition rate of 50 Hz, thus averaging over 3000 FEL shots. The fluctuation of the FEL intensity, on such timescales, is on the order of 5%.

The top panel of Fig. 2 shows the CCD image of the first all-EUV transient FWM signal. It was measured on a 50 nm thick Si_3N_4 membrane (Silson) at a fundamental wavelength of 54 nm, corresponding to a grating period of 113 nm. The associated wave vector mismatch $\Delta k = 9 \times 10^{-13}$ nm^{-1} is well compensated for by the ~10 nm attenuation length of Si_3N_4 at the fundamental wavelength, which results in $\beta = 0.999$, i.e., an almost ideally thin grating. The second harmonic signal is separated from the third harmonic one by 550 pixels, corresponding to an angular separation of 4.48°, well in agreement with the expected 4.56° separation. The bottom panel of Fig. 2 shows the same detector region when path 2 is blocked and the sample is exposed to pump 1 only. The absence of any scattered signal reveals its correlation to the presence of both pump arms.

To confirm that the observed signal is indeed FWM and quantify the magnitude of the response, the experiment was repeated as a function of the pump beam intensity on a 340 nm thick Si membrane (Norcada) at a fundamental wavelength $\lambda = 40$ nm and probe wavelength $\lambda_{\mathrm{pr}} = \lambda/3 = 13.3$ nm. This corresponds to an increased wave vector mismatch $\Delta k = 0.012$ nm^{-1}, which, associated with the 200 nm penetration depth of Si, results in $\beta = 0.6$. The FWM efficiency is defined as $\eta_{\mathrm{FWM}} = I_{\mathrm{FWM}}/I_3$, where I_{FWM} and I_3 are the intensities of the FWM and the probe signal, respectively.

Figure 3 shows the dependence of η_{FWM} as a function of the product of the pulse energies of pumps 1 and 2, which were varied simultaneously while keeping their ratio constant. It clearly exhibits the expected linear dependence on the product of the pump pulses, as indicated by the reported fit (red solid line), thus confirming the FWM nature of the signal.

The amplitude of the scattered FWM field is related to those of the pump fields as $E_{\mathrm{FWM}} \propto \chi^{(3)}_{\mathrm{eff}} E_1 E_2 E_3$, where $\chi^{(3)}_{\mathrm{eff}} = \sqrt{\eta_{\mathrm{FWM}}}/E_1 E_2$ can be considered an effective value for the $\chi^{(3)}$. Effective values for this quantity are typically reported in EUV and x-ray experiments with the aim of quantifying the magnitude of the nonlinear process. The determination of the real $\chi^{(3)}$ would require precise knowledge of experimental conditions—e.g., the intensity distribution across the wave front of the crossed pulses, which are not completely under control in these pioneering experiments. With pump electric field amplitudes on the order of 0.3×10^9 to 1.4×10^9 V m^{-1} and pump spot sizes of 4×10^4 μm^2, a value of $\chi^{(3)}_{\mathrm{eff}} \sim 6 \times 10^{-24}$ m^2 V^{-2} is extracted for the effective third-order susceptibility. As expected, the value of $\chi^{(3)}_{\mathrm{eff}}$ decreased by orders of magnitude compared to previous EUV-pump or optical probe TG experiments performed at FERMI that reported $\chi^{(3)}_{\mathrm{eff}} \sim 2 \times 10^{-20}$ m^2 V^{-2} [17]. However, this decrease is far less than the 8 orders of magnitude predicted by the simple anharmonic oscillator model [1]. This trend, similar to the one observed in previous experiments [17,30] is most probably due to resonance enhancement effects [2] since all photon energies are larger than the band gap of the material, thus leading to a significant electronic population in the conduction band continuum. Moreover, free-electron nonlinearities [31,32], similar to those that lead to NLO effects in plasmas, might become relevant at these photon energies, where the electron velocities due to the Lorentz force are comparable to those associated with the displacement in the anharmonic potential.

Our results demonstrate how a purely EUV FWM response with a significant efficiency can be detected in a real experiment, hence endorsing the feasibility of experiments so far only theoretically conceived. This represents a fundamental step forward in NLO and, together with the

previous results showing that EUV TG can drive coherent excitations in a solid sample [30] and with the ability of introducing a tunable pump-probe delay Δt already under commissioning at EIS-TIMER, constitutes the last step before effectively exploiting EUV TG to access excitation wave vectors in the range $\mathbf{k}_{ex} = 0.1$–$1\ \mathrm{nm}^{-1}$. Probing vibrations in this range, inaccessible both with the optical probe and with the most common scattering techniques [26], will be fundamental, e.g., to understand thermodynamic peculiarities of disordered and glassy systems [33,34]. Nevertheless, even the reported setup allows for unique experimental configurations at EUV or x-ray photon energies. In the first place, the signal beam retains the temporal and spatial coherence properties of the FEL emission and propagates along a well-defined, background-free direction. These are ideal properties for detection with a spectrometer which, combined with the fine tunability of the FERMI radiation, can be exploited for frequency domain FWM spectroscopy [35–37]. Second, it is possible to apply a tunable delay Δt_{exc} between the excitation pulses by acting on the mirrors of the beam line, and an additional pump-probe delay between the fundamental and the higher harmonics by acting on the machine configuration [24]. The latter can be tuned in the subfemtosecond regime with subattosecond resolution [24]. Thus, with the ability to fine-tune Δt and Δt_{exc}, the pump and probe central frequencies and the detection of the signal spectrum, the potential of the experiment goes well beyond a mere demonstrative exercise and opens the realm of EUV, element selective, multidimensional spectroscopy [38]. These novel kinds of spectroscopy can be applied, e.g., to the study of charge and energy transfer dynamics in light harvesting or emitting devices [6] or coherences between electronic, vibrational, and core levels [8]. The latter constitutes a unique possibility for the study of charge flows in biologically relevant molecules since all C, N, and O atoms have resonances in the EUV–soft x-ray energy range.

The authors acknowledge the European Research Council Grant No. 202804-TIMER.

*laura.foglia@elettra.eu

[1] R. W. Boyd, *Nonlinear Optics*, 3rd ed. (Elsevier Academic Press, New York, 2008).

[2] F. Bencivenga, S. Baroni, C. Carbone, M. Chergui, M. B. Danailov, G. De Ninno, M. Kiskinova, L. Raimondi, C. Svetina, and C. Masciovecchio, Nanoscale dynamics by short-wavelength four wave mixing experiments, New J. Phys. **15**, 123023 (2013).

[3] S. Tanaka, V. Chernyak, and S. Mukamel, Time-resolved x-ray spectroscopies: Nonlinear response functions and Liouville-space pathways, Phys. Rev. A **63**, 063405 (2001).

[4] B. Adams, Nonlinear X-ray optics: The next phase for X-rays, Nat. Phys. **7**, 675 (2011).

[5] K. Tamasaku, K. Sawada, E. Nishibori, and T. Ishikawa, Visualizing the local optical response to extreme ultraviolet radiation with a resolution of $\lambda/380$, Nat. Phys. **7**, 705 (2011).

[6] S. Tanaka and S. Mukamel, Coherent X-Ray Raman Spectroscopy: A Nonlinear Local Probe for Electronic Excitations, Phys. Rev. Lett. **89**, 043001 (2002).

[7] I. V. Schweigert and S. Mukamel, Double-quantumcoherence attosecond x-ray spectroscopy of spatially separated, spectrally overlapping core-electron transitions, Phys. Rev. A **78**, 052509 (2008).

[8] S. Mukamel, D. Healion, Y. Zhang, and J. D. Biggs, Multidimensional attosecond resonant x-ray spectroscopy of molecules: Lessons from the optical regime, Annu. Rev. Phys. Chem. **64**, 101 (2013).

[9] S. Shwartz, R. N. Coffee, J. M. Feldkamp, Y. Feng, J. B. Hastings, G. Y. Yin, and S. E. Harris, X-Ray Parametric Down-Conversion in the Langevin Regime, Phys. Rev. Lett. **109**, 013602 (2012).

[10] M. Beye, S. Schreck, F. Sorgenfrei, C. Trabant, N. Pontius, C. Schüßler-Langeheine, W. Wurth, and A. Föhlisch, Stimulated X-ray emission for materials science, Nature (London) **501**, 191 (2013).

[11] N. Rohringer, D. Ryan, R. A. London, M. Purvis, F. Albert, J. Dunn, J. D. Bozek, C. Bostedt, A. Graf, R. Hill, S. P. Hau-Riege, and J. J. Rocca, Atomic inner-shell X-ray laser at 1.46 nanometres pumped by an X-ray freeelectron laser, Nature (London) **481**, 488 (2012).

[12] K. Tamasaku, E. Shigemasa, Y. Inubushi, T. Katayama, K. Sawada, H. Yumoto, H. Ohashi, H. Mimura, M. Yabashi, K. Yamauchi, and T. Ishikawa, X-ray two-photon absorption competing against single and sequential multiphoton processes, Nat. Photonics **8**, 313 (2014).

[13] M. Fuchs *et al.*, Anomalous nonlinear X-ray Compton scattering, Nat. Phys. **11**, 964 (2015).

[14] S. Shwartz, M. Fuchs, J. B. Hastings, Y. Inubushi, T. Ishikawa, T. Katayama, D. A. Reis, T. Sato, K. Tono, M. Yabashi, S. Yudovich, and S. E. Harris, X-Ray Second Harmonic Generation, Phys. Rev. Lett. **112**, 163901 (2014).

[15] T. E. Glover, D. M. Fritz, M. Cammarata, T. K. Allison, S. Coh, J. M. Feldkamp, H. Lemke, D. Zhu, Y. Feng, R. N. Coffee, M. Fuchs, S. Ghimire, J. Chen, S. Shwartz, D. A. Reis, S. E. Harris, and J. B. Hastings, X-ray and optical wave mixing, Nature (London) **488**, 603 (2012).

[16] F. Bencivenga, R. Cucini, F. Capotondi, A. Battistoni, R. Mincigrucci, E. Giangrisostomi, A. Gessini, M. Manfredda, I. P. Nikolov, E. Pedersoli, E. Principi, C. Svetina, P. Parisse, F. Casolari, M. B. Danailov, M. Kiskinova, and C. Masciovecchio, Four-wave mixing experiments with extreme ultraviolet transient gratings, Nature (London) **520**, 205 (2015).

[17] F. Bencivenga *et al.*, Four-wave-mixing experiments with seeded free electron lasers, Faraday Discuss. **194**, 283 (2016).

[18] S. Mukamel, *Principles of Nonlinear Optics and Spectroscopy* (Oxford University Press, New York, 1995).

[19] E. Allaria *et al.*, Highly coherent and stable pulses from the FERMI seeded free-electron laser in the extreme ultraviolet, Nat. Photonics **6**, 699 (2012).

[20] E. Allaria *et al.*, Two-stage seeded soft-X-ray freeelectron laser, Nat. Photonics **7**, 913 (2013).

[21] E. Allaria *et al.*, Control of the Polarization of a Vacuum-Ultraviolet, High-Gain, Free-Electron Laser, Phys. Rev. X **4**, 041040 (2014).

[22] E. Ferrari *et al.*, Widely tunable two-colour seeded free-electron laser source for resonant-pump resonant-probe magnetic scattering, Nat. Commun. **7**, 10343 (2016).

[23] F. Bencivenga, F. Capotondi, F. Casolari, F. Dallari, M. B. Danailov, G. De Ninno, D. Fausti, M. Kiskinova, M. Manfredda, C. Masciovecchio, and E. Pedersoli, Multi-colour pulses from seeded free-electron-lasers: towards the development of non-linear core-level coherent spectroscopies, Faraday Discuss. **171**, 487 (2014).

[24] K. C. Prince *et al.*, Coherent control with a shortwavelength free-electron laser, Nat. Photonics **10**, 176 (2016).

[25] R. Cucini, F. Bencivenga, M. Zangrando, and C. Masciovecchio, Technical advances of the TIMER project, Nucl. Instrum. Methods Phys. Res., Sect. A **635**, S69 (2011).

[26] F. Bencivenga and C. Masciovecchio, FEL-based transient grating spectroscopy to investigate nanoscale dynamics, Nucl. Instrum. Methods Phys. Res., Sect. A **606**, 785 (2009).

[27] F. Bencivenga and C. Masciovecchio, Results and perspectives for short-wavelength, four-wave-mixing experiments with fully coherent free electron lasersSynchrotron Radiat. News **29**, 15 (2016).

[28] L. Foglia, F. Bencivenga, R. Mincigrucci, A. Simoncig, A. Calvi, R. Cucini, E. Principi, M. Zangrando, N. Mahne, M. Manfredda, L. Raimondi, E. Pedersoli, F. Capotondi, M. Kiskinova, and C. Masciovecchio, Four-wave-mixing experiments and beyond: the TIMER/mini-TIMER setups at FERMI, Proc. SPIE Int. Soc. Opt. Eng. **10237**, 102370C (2017).

[29] M. Zangrando, D. Cocco, C. Fava, S. Gerusina, R. Gobessi, N. Mahne, E. Mazzucco, L. Raimondi, L. Rumiz, and C. Svetina, Recent results of PADReS, the photon analysis delivery and REduction system, from the FERMI FEL commissioning and user operations, J. Synchrotron Radiat. **22**, 565 (2015).

[30] F. Bencivenga, R. Cucini, F. Capotondi, A. Battistoni, R. Mincigrucci, E. Giangrisostomi, A. Gessini, M. Manfredda, I. P. Nikolov, E. Pedersoli, E. Principi, C. Svetina, P. Parisse, F. Casolari, M. B. Danailov, M. Kiskinova, and C. Masciovecchio, Advances in X-ray free-electron lasers instrumentation III, Proc. SPIE Int. Soc. Opt. Eng. **9512**, 951212 (2015).

[31] N. Bloembergen, R. K. Chang, S. S. Jha, and C. H. Lee, Optical second-harmonic generation in reection from media with inversion symmetry, Phys. Rev. **174**, 813 (1968).

[32] S. Yudovich and S. Shwartz, Second-harmonic generation of focused ultrashort x-ray pulses, J. Opt. Soc. Am. B **32**, 1894 (2015).

[33] W. Schirmacher, B. Schmid, C. Tomaras, G. Viliani, G. Baldi, G. Ruocco, and T. Scopigno, Vibrational excitations in systems with correlated disorder, Phys. Status Solidi (c) **5**, 862 (2008).

[34] C. Ferrante, E. Pontecorvo, G. Cerullo, A. Chiasera, G. Ruocco, W. Schirmacher, and T. Scopigno, Acoustic dynamics of network-forming glasses at mesoscopic wavelengths, Nat. Commun. **4**, 1793 (2013).

[35] S. Mukamel and R. F. Loring, Nonlinear response function for time-domain and frequency-domain four-wave mixing, J. Opt. Soc. Am. B **3**, 595 (1986).

[36] R. M. Hochstrasser, Two-dimensional spectroscopy at infrared and optical frequencies, Proc. Natl. Acad. Sci. U.S.A. **104**, 14190 (2007).

[37] D. B. Turner, P. C. Arpin, S. D. McClure, D. J. Ulness, and G. D. Scholes, Coherent multidimensional optical spectra measured using incoherent light, Nat. Commun. **4**, 2298 (2013).

[38] S. T. Cundiff and S. Mukamel, Optical multidimensional coherent spectroscopy, Phys. Today **66**, No. 7, 44 (2013).